Hamiltonian scattering chaos in a hydrodynamical system

1992 J. Phys. A: Math. Gen. 25 3929

(http://iopscience.iop.org/0305-4470/25/14/012)

J. Phys. A: Math. Gen. 25 (1992) 3929-3943. Printed in the UK

Hamiltonian scattering chaos in a hydrodynamical system

C Jung† and E Ziemniak‡

† Fachbereich Physik, Universität Bremen, 2800 Bremen, Federal Republic of Germany
‡ Ruhr-Universität Bochum, 4630 Bochum, Federal Republic of Germany

Received 17 December 1991, in final form 23 March 1992

Abstract. The dynamics of chaotic scattering in Hamiltonian phase space can be visualized by two-dimensional open hydrodynamical systems with velocity fields, which are periodic in time. Passive marker particles in the fluid trace out complicated trajectories, which are caused by the vortex structure of the fluid; i.e. we encounter a case of Lagrangian turbulence. By the examination of a particular model we show the applicability in hydrodynamics of ideas and methods which have been useful before in the investigation of systems describing chaotic particle scattering. In particular we show the existence of a chaotic saddle, show its influence on scattering trajectories and give some quantitative measures for it.

1. Introduction

In recent years there has been a growing interest in the phenomenon of chaotic scattering (for reviews see [1, 2]). In classical dynamics chaotic scattering is created by the following mechanism: in phase space there is an infinite set of unstable localized orbits, periodic orbits of arbitrarily long periods and truly chaotic unperiodic orbits. This set of localized orbits occupies a subset of measure zero in the phase space only. It is called a chaotic saddle Λ. The stable manifolds of orbits of Λ reach out into the incoming asymptotic region. Whenever a scattering trajectory starts exactly on such a stable manifold, it converges towards a localized orbit and will never reach the outgoing asymptotic region; it gets stuck in the interaction zone. This happens for a subset of initial scattering conditions of measure zero only. All other initial conditions lead to generic scattering trajectories having a proper outgoing asymptote. However, generic scattering trajectories will run besides the chaotic localized orbits for a finite time and the whole stream of incoming particles casts a kind of shadow image of Λ into the outgoing aymptotic region. So it is possible to reconstruct important properties of Λ from scattering measurements. In particular, the scattering functions like the deflection function or the the time delay function have singularities on a fractal subset of their domain and so they reflect the fractal structure of Λ. With this picture in mind we *interpret scattering chaos as the Hamiltonian version of transient chaos* [3].

These are the fundamentals of classical scattering chaos. However, particle scattering experiments are done with microscopic systems mainly, where quantum effects are essential. In quantum dynamics the whole concept of chaos is less well defined than in classical dynamics. Therefore, in order to be able to study the basic mechanism of chaotic scattering it would be desirable to have a truly classical situation where we can observe the mechanism of scattering chaos at work. The motion of macroscopic rigid bodies is not well suited to this purpose because friction destroys the Hamiltonian character of the dynamics. In addition, the main events of classical mechanics happen

0305-4470/92/143929+15$04.50

not in position space but in phase space and there the trajectories are not displayed directly before our eyes.

Therefore it would be useful to have a system where we have visualized the phase space motion of classical scattering chaos directly. In this paper we explain and demonstrate by model computations that hydrodynamical systems are able to realize this idea. Our visualization of Hamiltonian scattering chaos by an open hydrodynamical system goes along similar patterns to the visualization of bound Hamiltonian chaos by hydrodynamical systems in a closed box as explained in [4, 5]. Two previous examples of chaotic advection in open hydrodynamical systems and some relations to chaotic scattering can be found in [6, 7].

The aim of this paper is to treat a particular hydrodynamical system (the flow through a channel with an obstacle) like a system of particle scattering and to apply to it the methods which we have used before in the description of chaotic particle scattering [8–11].

2. A hydrodynamical model for chaotic particle scattering

Consider a channel of finite width W and infinite length and disregard the third dimension, i.e. let us consider a system in two-dimensional position space. The coordinate along the channel is x, the coordinate in transverse direction is y. Inside the channel we place a circular obstacle, the cylinder, with radius R. An incompressible viscid fluid is pumped through the channel from the left to the right. We assume that the velocity of the fluid is sufficiently small such that far away in front and far away behind the cylinder a parabolic velocity profile is created. Only in the direct vicinity behind the cylinder we find a more complicated flow pattern which depends sensitively on the Reynolds number Re or on the viscosity of the fluid. For a small value of Re the flow becomes stationary in the long time limit. For a large value of Re the velocity field has a very complicated pattern which is irregular in time. In the following we concentrate on the range of Reynolds numbers in between, where an exactly time-periodic flow occurs. Behind the cylinder vortices are created, which detach from the cylinder and drift down the channel. After some distance they are destroyed by viscosity. We obtain a typical Karman vortex street of finite length.

Because of the exact periodicity in time the velocity field cannot be chaotic and we do not encounter turbulence of the velocity field. In this paper we are interested in the study of trajectories of passive marker particles swimming in the given flow. If the particles come in sufficiently far away from the middle of the channel, then they do not enter the vortex street, they stay in the strip between the vortex street and the wall of the channel. Such particles are little affected by the obstacle and pass it quite rapidly. However, if the particles come in close to the middle of the channel, then they enter the vortex street directly and are whirled around inside the vortices for some time. Only a subset of initial conditions of measure zero leads to permanent trapping of the particles in the vicinity of the cylinder. Almost all particles escape after some time and reach the outgoing asymptotic region, where the motion becomes simple again. This temporary trapping of particles and the corresponding temporarily complicated motion between the trivial initial and trivial final motion is typical for scattering chaos or transient chaos.

The complicated motion in the vicinity of the cylinder is organized around some unstable periodic orbits. A transiently chaotic particle trajectory approaches the vicinity

of some unstable periodic orbit along its stable manifold, runs beside it for a while, switches to the vicinity of some other unstable periodic orbit via a heteroclinic connection between these two periodic orbits, stays with this second periodic orbit for a while etc until finally it is released into the outgoing asymptotic region along the unstable manifolds of the periodic orbits. In the rest of this paper we shall work out and explain these ideas in more detail.

Let us begin by specifying the geometrical arrangement. We choose the unit of length such that the width W of the channel has the value $W = 0.2$. For the radius of the cylinder we choose $R = 0.05$. The cylinder is located in the middle of the channel and the zero of the x-axis is chosen such that the centre of the cylinder has the coordinates $(x_c, y_c) = (0.25, 0.1)$. This arrangement is plotted in figure 1.

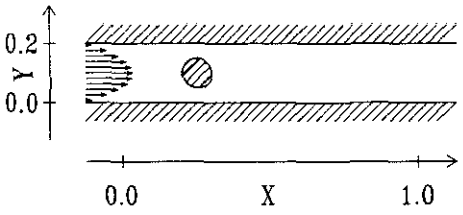

Figure 1. Geometry of the channel and the cylinder in it. The arrows inside the channel indicate the incoming parabolic velocity profile.

The fluid comes in with a parabolic velocity profile as indicated in the figure. More precisely: let the velocity components of the fluid in x and y direction be u and v respectively. We assume that for $x \ll x_c = 0.25$ and for $x \gg x_c = 0.25$ we have

$$u(x, y) = u_0 y(0.2 - y) \tag{1}$$

$$v(x, y) \equiv 0 \tag{2}$$

and u_0 has been given the value $u_0 = 6/W^2$ such that the total incoming flow $\int_0^W u(x, y)\, dy = W$, i.e. the mean velocity u_{av} equals 1. In the numerical solutions of the Navier-Stokes equation it turns out that the parabolic velocity profile is valid rather close to the cylinder and so it was sufficient for the following to choose as initial condition this profile along the line $x = 0.0$.

The Navier-Stokes equation has been solved numerically by a functional method described in detail in [12]. In all the following numerical computations the value $Re = 80$ is chosen, which is close to the lower boundary of the interval of periodic behaviour. This value of Re is based on the mean velocity and the diameter of the cylinder. For this value of Re the cycle time of the periodic solution has the value $T_c = 1.109$. Here the unit of time is given by the quotient between the unit of length and u_{av}. Such a relatively small value of Re (large value of the viscosity) has the advantage, that at $x = 1.0$ the velocity profile comes close again to the parabolic profile given in equations (1) and (2). In the terminology of scattering theory at $x = 1.0$ the outgoing asymptotic region is already reached and we can restrict the numerical computations to the x-interval $x \in [0.0, 1.0]$. In particular, all vortices created behind the cylinder are damped out at $x \approx 0.6$.

Because of the reflectional symmetry in the line $y = 0.1$ of the geometrical arrangement of the channel, the velocity field has the following symmetry:

$$u(x, y, t) = u(x, W - y, t + T_c/2) \tag{3}$$

$$v(x, y, t) = -v(x, W - y, t + T_c/2). \tag{4}$$

Because of the incompressibility of the fluid there exists a function $\psi(x, y, t)$ such that

$$u(x, y, t) = \frac{\partial}{\partial y}\psi(x, y, t) \tag{5}$$

$$v(x, y, t) = -\frac{\partial}{\partial x}\psi(x, y, t) \tag{6}$$

for all x, y, t. The level lines of ψ for fixed t are the stream lines of the flow. Figure 2(a) gives a plot of the stream lines at time $t = 0 \bmod T_c$, where we have chosen the zero of time arbitrarily. If the velocity field were stationary, then the stream lines would coincide with the trajectories of the fluid particles. Figure 2(b) shows the stream lines at a time $t = T_c/4 \bmod T_c$.

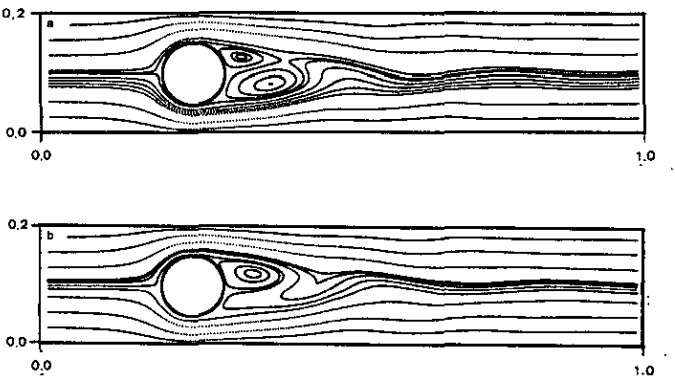

Figure 2. Stream lines of the flow at time t, where $t = 0$ in part (a), and $t = T_c/4$ in part (b).

From figures 2 and the symmetry properties of the flow we can imagine the time development of the velocity field. Behind the cylinder vortices are created, two in number within any time interval of length T_c, one in the upper half and the other one in the lower half of the channel delayed by a time $T_c/2$. The vortices first grow in size, then they become detached from the cylinder and start to drift along the channel. Now the viscosity of the fluid becomes important for their destabilization and destruction after a short length of travel.

Next consider a passive marker particle which is placed into the fluid at time $t = t_{in}$ in position $x = x_{in}$, $y = y_{in}$ and let it swim with the fluid through the channel. The trajectory of this particle is the solution of the following equations of motion:

$$\frac{d}{dt}x(t) = u(x, y, t) = \frac{\partial}{\partial y}\psi(x, y, t) \tag{7}$$

$$\frac{d}{dt}y(t) = v(x, y, t) = -\frac{\partial}{\partial x}\psi(x, y, t) \tag{8}$$

with the initial conditions $x(t_{in}) = x_{in}$, $y(t_{in}) = y_{in}$. Equations (7) and (8) have exactly the same structure as the Hamiltonian equations of motion for a particle moving along a one-dimensional position space under the influence of an explicitly time-dependent force. We have to make the following identifications: $x \to q$ where q is the position of

the particle, $y \to p$ where p is the canonically conjugate momentum of the particle, $\psi(x, y, t) \to H(q, p, t)$ where H is the explicitly time-dependent Hamiltonian function of the dynamics. Accordingly, the plot of the stream lines as shown in figure 2 can also be interpreted as the level lines of the Hamiltonian function at fixed time. For $x \to -\infty$ or $x \to +\infty$, ψ does not really depend on either x or on t, but on y only. In the same way for $q \to -\infty$ or $q \to +\infty$, H does not depend on either q or on t, but on p only. Therefore, asymptotically the particle moves with constant speed and we can view the limit $q \to \pm\infty$ or $x \to \pm\infty$ as the asymptotic limit of scattering theory.

It is well known that explicitly time-dependent Hamiltonian systems with one degree of freedom can show chaotic behaviour of essentially the same type as autonomous systems with two degrees of freedom. If the system is open as in the case of our present model system, then almost all trajectories come in from the incoming asymptotic region, they may exhibit complicated motion for a finite time in the region in which the dynamics is really time dependent, and disappear again into the outgoing asymptotic region. If the dynamics is chaotic at all, then we expect to see transient chaos or scattering chaos. In [11] an example for scattering chaos in an explicitly time-dependent one-dimensional system, namely the periodically driven Morse system, has been analysed in detail. In the present paper we shall show that our hydrodynamical system provides an example of essentially the same type of transient chaos via the analogy between the hydrodynamical flow in a two-dimensional position space and the Hamiltonian flow in the two-dimensional phase space.

For a scattering system it is essential, to give a proper labelling of asymptotes. In our model system this can be done as follows: pick a particular value x_{in} of x in the incoming asymptotic region (in our examples we shall take $x_{in} = 0.02$) and record the y-coordinate and the time modulo T_c at which the trajectory crosses the line $x = x_{in}$. These two numbers y_{in} and t_{in} label any incoming asymptote uniquely.

3. Time delay function

A clear criterion for transient chaos is the occurrence of a fractal set of singularities in the time delay function [3]. In our system this means in detail: take a one-dimensional subset of initial asymptotes e.g. fix y_{in}, scan t_{in} and plot the time Dt which the particle needs to reach the outgoing asymptotic region, e.g. the line $x = 1.0$. If the system contains transient chaos, then for appropriately chosen values of y_{in} this function has infinities on a fractal set along the t_{in}-axis and it has intervals of continuity in-between in the gaps of the fractal set.

Figure 3(a) displays a representative example of Dt as function of t_{in}, namely the example for $y_{in} = 0.0995$. We see smooth parts and places where the function shows rapid changes, which are not well resolved on this scale. Figure 3(b) gives a magnification with improved resolution of a part of figure 3(a) which contains places of complicated behaviour of the function $Dt(t_{in})$. Between the long intervals of continuity there appear shorter intervals of continuity, in which the values of Dt are significantly higher. However, these smaller intervals do not fill up the whole axis, in-between there still remain small unresolved intervals of complicated behaviour. In the unresolved regions this behaviour under magnification continues forever. We see a typical Cantor set construction: on any level of the hierarchy there are intervals of continuity and unresolved complements in-between. On the next level we find new intervals of continuity inside the so far unresolved parts. After every step of this construction there

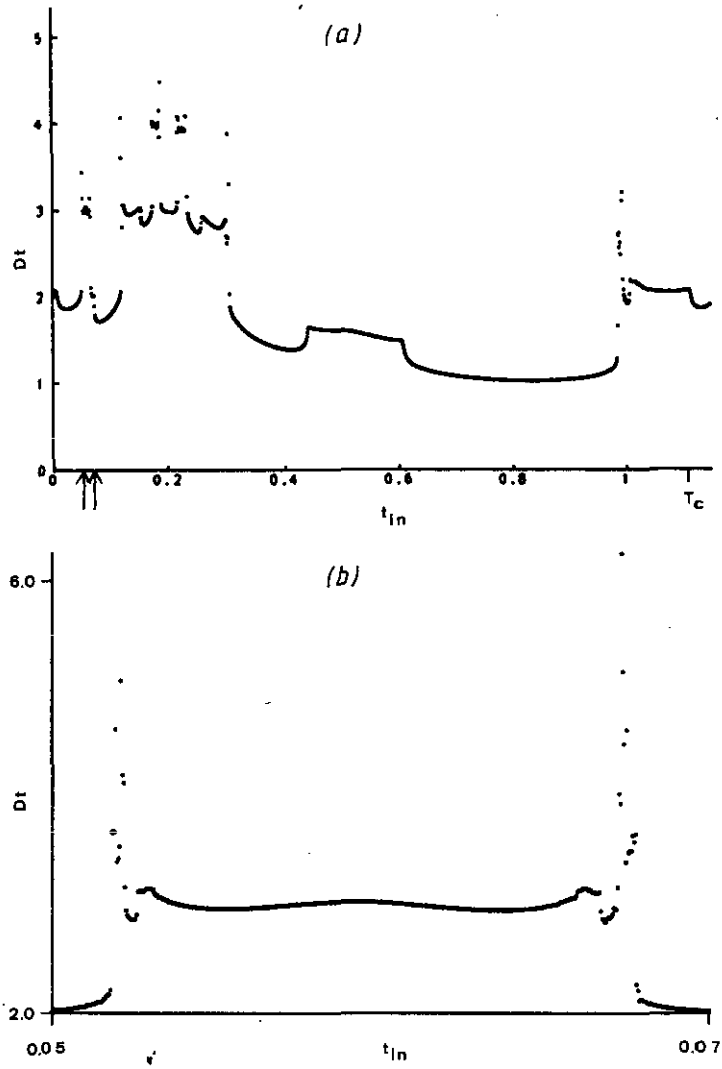

Figure 3. Plot of the function $Dt(t_{in})$ for $y_{in} = 0.0995$. Part (a) shows this function on its whole domain. Part (b) shows a magnification in one of the small intervals containing singularities. The boundaries of the t_{in} interval of part (b) are marked by arrows in part (a).

remain even more smaller unresolved parts than in the previous step. The Cantor set itself is the set of accumulation points of the boundaries of intervals of continuity. From level to level in this hierarchy the value of Dt increases and on the Cantor set itself the function Dt goes to infinity.

A first clue to the mechanism behind this phenomenon can be obtained by an inspection of particle trajectories whose incoming asymptotes belong to different intervals of continuity. Figure 4 provides some examples for $y_{in} = 0.0995$ and different values of t_{in} as indicated in the figure caption. The plots of the trajectories consist of a sequence of points along it such that the time separation between adjacent points is $T_c/100$. In part (a) we see a trajectory of a particle which needs only a short time to travel through the channel and which runs through quite straight. In contrast, the

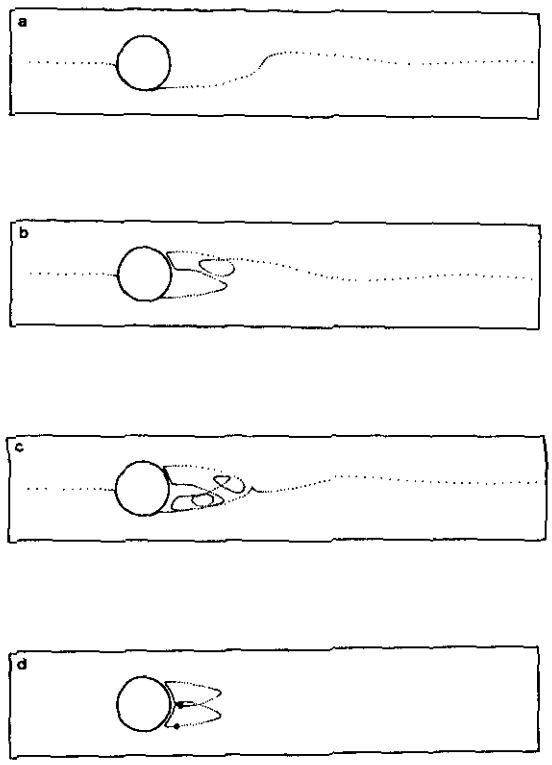

Figure 4. Some particle trajectories in position space. Parts (a, b, c) show scattering trajectories with $y_{in} = 0.0995$ and $t_{in} = 0.4$ in part (a), $t_{in} = 0.121\,404$ in part (b), and $t_{in} = 0.121\,4815$ in part (c). The values of Dt for these trajectories are 1.39, 3.54, 5.12 respectively. Part (d) shows the simplest and most important periodic orbits of the system. The position of the particles on these periodic orbits at time $t = 0.3$ mod T_c are marked by open circles. These points are the fixed points r and $\bar{r}$ of the stroboscopic map taken at time $T_M = 0.3$. The trajectories are represented by a sequence of points which give the position of the particle after each time step of length $T_c/100$. The frames are $x \in [0.0, 1.0]$, $y \in [0.0, 0.2]$ as in figure 2.

trajectory in part (b), whose initial condition belongs to a smaller interval, traces out a longer and more complicated path containing loops. Accordingly it needs a longer time to reach the outgoing asymptotic region. Part (c) shows a very long and complicated trajectory starting in an even smaller interval. It contains many loops behind the cylinder because the marker particle gets trapped by the vortices sitting there for a while before it is freed again and continues its journey along the channel.

Now we explain the structure of the time delay function in terms of the influence of the cylinder and of the vortices on the particle motion. In a very coarse approximation we can disregard all fine structure of this function, i.e. remove all small intervals with high values of Dt and in particular all singularities. There remains a sawtooth function of the following shape: there is a linear part $Dt = c - t_{in}$ in the interval $t_{in} \in (0, 0.99\ldots)$ and a linear part $Dt = c - t_{in} + T_c$ in the interval $t_{in} \in (0.99\ldots, T_c)$. If we consider that $t_{in} = 0$ and $t_{in} = T_c$ have to be identified, then we have just one single straight line of slope -1 reaching from $T_j + \varepsilon$ to $T_j - \varepsilon$, where the point of jump $T_j \approx 0.99\ldots$; i.e. in highest order of the fractal hierarchy the Dt function is described by a sawtooth

function with a jump of height T_c at $t_{in} = T_j$ and a slope of -1 otherwise. This can be interpreted in terms of the particle trajectories as follows: if the particle starts its motion at $t_{in} = T_j - \varepsilon$ then it passes the vicinity of the cylinder in the shortest possible time. If it starts at some earlier time $t_{in} = T_j - \tau$ then in the vicinity of the cylinder the particle waits for a time τ until the velocity field of the fluid has reached the same state as for the former trajectory. If the particle starts at time $t_{in} = T_j + \varepsilon$ then it has to wait for nearly a whole period T_c at the cylinder before it can continue its journey. This behaviour indicates that behind the cylinder the particle is trapped until a new vortex is created on the appropriate side and detaches from the cylinder transporting the particle away within it.

If the particle stays attached to this vortex, then it is taken away and as soon as the vortex is destroyed by viscosity further down the channel, the particle finds itself in the laminar asymptotic flow. This is the complete fate for all particles with small values of Dt whose trajectories belong to the long intervals of continuity in figure 3.

For small intervals of appropriate initial conditions the particle does not stay with the same vortex but switches from one particular vortex to another one by the following mechanism: in time-independent velocity fields, the particle trajectories coincide with the stream lines for fixed time. Then it would be impossible for a particle ever to enter a vortex from outside or to leave it from inside. However, when the velocity field is time dependent, the position of the vortices changes against the particle and the particle can be overrun by a vortex and come inside of it. After a while the particle may be left behind the vortex again. If it leaves one vortex at just the appropriate time and at the right place, then it may be overrun by the next vortex and be trapped by it for a while, etc. So a particle can be handed over from one vortex to the next one and stay in the region behind the cylinder for a long time, even though each individual vortex leaves this region quite soon. For this effect to occur, it is necessary that the particle motion is synchronized to the vortex motion such, that inside the growing and moving vortex the particle is moved from the front, where it is captured, to the rear, where it is released again. Thereby the particle is set back in position space by a diameter of a vortex relative to the moving vortex itself. Accordingly, for every time a particle changes from one vortex to the next one, it is delayed by approximately $T_c/2$ when it switches between consecutive vortices on different sides of the cylinder and by approximately T_c when it switches between successive vortices on the same side. Those small intervals of initial conditions which allow for this mechanism to occur are the positions of the higher and smaller structures in figure 3. Of course, the longer a particle is supposed to remain trapped, the more precise the initial conditions of its incoming asymptote must be selected. Only for a subset of initial conditions of measure zero can the particle be trapped forever.

A temporarily trapped scattering trajectory simulates the motion of localized orbits behind the cylinder. Therefore, in order to understand the complicated behaviour of long scattering trajectories, it is necessary to study the properties of periodic and localized orbits in the system. The simplest truly periodic orbits are plotted in figure 4(d). The upper one will be called γ in the following and the lower one will be called $\tilde{\gamma}$. They are related by the symmetries (3, 4) and the time of revolution is exactly T_c for both of them. They are unstable and they form the backbone of the transient chaos as will be evident in the next section. A particle revolving around γ or around $\tilde{\gamma}$ is handed over from each vortex on one side of the cylinder to the next vortex on the same side indefinitely and it traces out just one loop in each member of this infinite sequence of vortices.

4. Stroboscopic map

Now we use some methods and the terminology of nonlinear dynamics without explaining them in detail. The reader not familiar with these issues and their applications to chaotic advection may consult the textbooks [13, 14] and the review articles [15, 16].

Next we give some information on the orbits γ and $\tilde{\gamma}$ by the study of the stroboscopic map taken for times $t = T_M \bmod T_c$ where we have chosen $T_M = 0.3$. The orbits γ and $\tilde{\gamma}$ correspond to two fixed points r and $\tilde{r}$ of this map. These two points are inverse hyperbolic and their eigenvalues are $\mu_1 = 1/\mu_2 \approx -80$.

By $W^u(r)$, $W^s(r)$, $W^u(\tilde{r})$, $W^s(\tilde{r})$ we denote the unstable and stable manifolds of r and $\tilde{r}$ respectively. Figure 5 shows the positions of the fixed points r and $\tilde{r}$ and some points of their stable and unstable manifolds in the stroboscopic plane. Because of numerical reasons we cannot show the complete invariant manifolds in their infinite length having an infinite number of tendrils but only a finite number of points of them.

Part (a) of figure 5 gives the unstable manifolds $W^u(r)$ and $W^u(\tilde{r})$, part (b) gives the stable manifolds $W^s(r)$ and $W^s(\tilde{r})$. Part (c) shows all these manifolds in a smaller region of the stroboscopic plane. In part (c) adjacent points have been connected to result in continuous lines. Most important, in figure 5(c) are the homoclinic and heteroclinic intersections of the invariant manifolds. They imply the existence of an infinite number of unstable periodic points of M with arbitrarily long period and an overcountable number of unperiodic truly chaotic points, whose trajectories are localized, i.e. the x coordinate of all iterated images and pre-images does not leave the region directly behind the cylinder. All these localized orbits taken together form the chaotic saddle Λ and they all have their stable and unstable manifolds reaching out

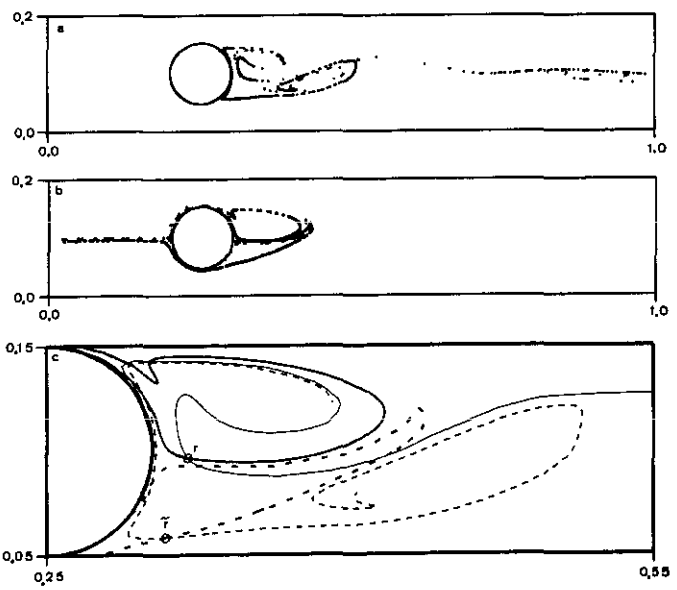

Figure 5. The fixed points r and $\tilde{r}$ (marked by open circles in part (c)) and some pieces of their invariant manifolds in the stroboscopic plane for $T_M = 0.3$. Part (a) gives the unstable manifolds, part (b) gives the stable manifolds. Part (c) shows the initial segments of the stable and the unstable manifolds including a few homoclinic and heteroclinic intersections. In part (c), $W^s(r)$ is represented by the thick solid line, $W^u(r)$ by the thin solid line, $W^s(\tilde{r})$ by the thick broken line, and $W^u(\tilde{r})$ by the thin broken line.

into the asymptotic region running essentially parallel to the invariant manifolds of r and $\tilde{r}$.

Figure 6 shows two of the trajectories belonging to some homoclinic and heteroclinic points of figure 5(c). In figure 6(a) we see a heteroclinic trajectory. It converges towards γ for $t \to +\infty$ and towards $\tilde{\gamma}$ for $t \to -\infty$. The middle part of this heteroclinic trajectory (i.e. the segment represented by the sequence of crosses) gives an impression of how a particle is handed over from one vortex to the next vortex on the other side of the cylinder. Before and after this solitary crossing over, the particle on the heteroclinic trajectory always remains on one side of the cylinder. Figure 6(b) presents a homoclinic trajectory. For $t \to -\infty$ as well as for $t \to +\infty$ it converges towards γ. Figure 6(b) illustrates the mechanism by which a particle can increase its delay time by the value T_c while it stays close to the cylinder. Along this homoclinic trajectory the particle circles around the periodic trajectory γ many times, then it leaves γ temporarily, it comes closer to the cylinder and within the next time interval of length T_c it moves upwards close to the wall of the cylinder with very small velocity. Finally it comes back to γ and continues to circle around it. In the long run the particle on this homoclinic trajectory has made one revolution less than a particle which stays on γ always.

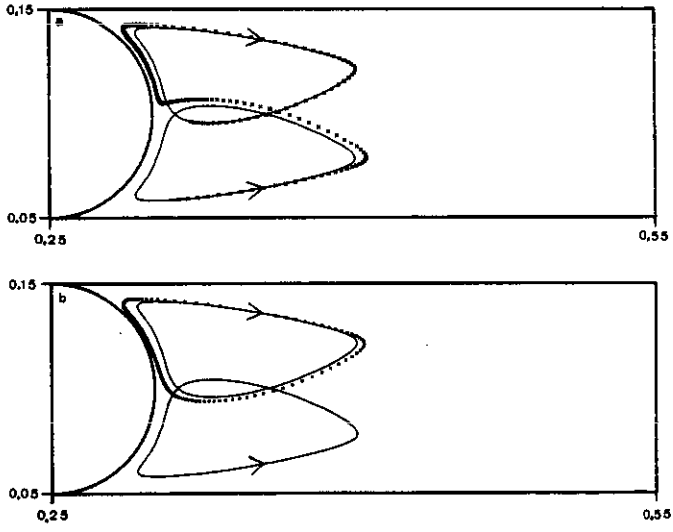

Figure 6. Part (a) shows a heteroclinic trajectory (marked by crosses), which switches from $\tilde{\gamma}$ to γ (these periodic orbits are drawn as solid lines). Part (b) shows a homoclinic trajectory to the periodic orbit γ. The arrows indicate the orientation of motion.

Scattering trajectories are complicated and have a large time delay when they come close to localized orbits of Λ, i.e. when they start close to stable manifolds of Λ. Therefore a knowledge of the location of these stable manifolds in the initial asymptotic region explains the pattern of the singularities in the time delay function. Experience with other systems has shown that the bundle of invariant manifolds of a chaotic saddle is locally the Cartesian product of lines with a Cantor set. The manifolds of any particular periodic point of the saddle are placed in this bundle in such a way that the topological closure of this subset contains the whole bundle. So we can choose the manifolds of the most simple periodic points (they are r and $\tilde{r}$ in our case) to

represent the structure of all the invariant manifolds of Λ. Next the intersection of $W^s(r)$ and $W^s(\tilde{r})$ with the plane of incoming asymptotes is constructed in order to indicate which initial conditions lead to trajectories coming close to localized orbits: we take points on $W^s(r)$ and $W^s(\tilde{r})$, construct the corresponding trajectories, run them backwards in time until they intersect the line $x = 0.02$. At this moment we record the values of y and t mod T_c and plot these values into the asymptotic plane to obtain figure 7. Again we can only show a finite number of points of a structure which really consists of a fractal pattern of lines wound up to an infinite number of tendrils. The stable manifolds of all other periodic orbits intersect this plane in lines running close to the ones coming from γ and $\tilde{\gamma}$; i.e. the stable manifolds of all orbits of Λ intersect the incoming asymptotic plane in a fractal arrangement of lines which is well represented by the contributions from γ and $\tilde{\gamma}$ only. The obvious symmetry of figure 7 is caused by the symmetry (3, 4) of the velocity field.

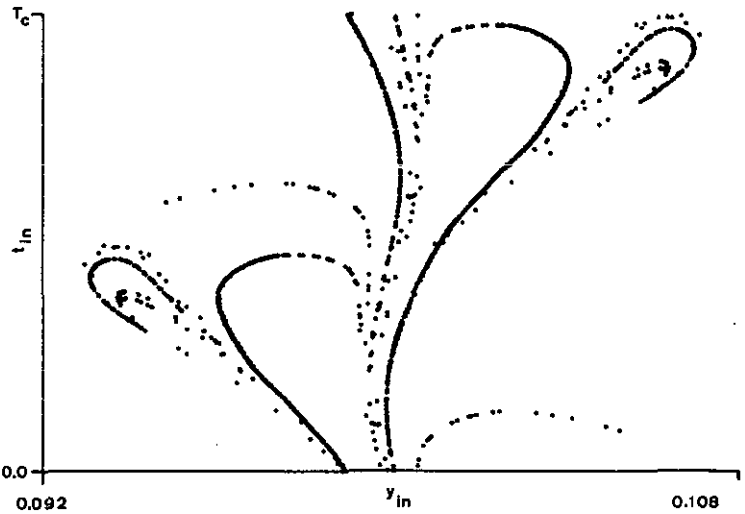

Figure 7. Intersection of the stable manifolds of γ and $\tilde{\gamma}$ with the initial asymptotic plane.

Now we are ready to understand the occurrence of the complicated behaviour of the system: whenever an initial condition of an incoming scattering trajectory lies exactly on a stable manifold of a localized orbit, then this scattering trajectory converges towards this localized orbit and gets trapped in the region behind the cylinder. Of course, this can only happen for a subset of initial conditions which has measure zero in the set of all initial conditions. When the scattering trajectory starts close to stable manifolds of Λ but not exactly on top of them, then it comes close to localized orbits and runs along orbits of Λ for a finite time. The closer the trajectory starts to stable manifolds, the longer it will run in the neighbourhood of orbits of Λ and the longer it takes until it finds its way out of the region directly behind the cylinder. If the initial conditions of two scattering trajectories are arbitrarily close to each other but lie on different sides of a stable manifold, then these two trajectories look similar until they come close to the localized orbit belonging to this stable manifold. They pass this localized orbit on different sides and from then on these two scattering trajectories show qualitatively different behaviour and their total time-of-flight can differ by a large amount. Because of the chaotic saddle, there is a fractal arrangement of dividing

unstable periodic orbits and a small bundle of incoming scattering trajectories can be split into an infinite number of sub-bundles which all behave qualitatively different. This is the scattering version of the sensitive dependence on initial conditions, which is a criterion for chaos.

Because of the existence of heteroclinic connections the scattering trajectories can switch from the neighbourhood of one periodic orbit to the neighbourhood of another one and visit the vicinities of several periodic orbits in a great variety of orders. By this arbitrary switching the trajectories of the completely deterministic system can realize random sequences. Generic scattering trajectories having proper in and out asymptotes can trace out sequences of finite length only. Those trajectories of measure zero, which get stuck in the interaction zone, can realize one-sided infinite sequences. Only the chaotic localized orbits belonging to Λ can realize two-sided infinite sequences.

If we take the line L defined by $y = 0.0995$ in figure 7, then we pick out the initial conditions used in figure 3. A comparison shows that the intersection between L and the stable manifolds of Λ mark those values of t_{in} at which Dt becomes large. Figure 7 provides an overview, for which values of y_{in} singularities of the function $Dt(t_{in})$ are to be expected. They occur for $y_{in} \in I_c = [0.093 \ldots, 0.107 \ldots]$, i.e. for values of y_{in} such that the line of constant y_{in} intersects the stable manifolds of Λ. In particular, for initial values of y_{in} outside of I_c the particles never show chaotic motion. They pass the region behind the cylinder quite straight and sufficiently close to the wall in order to be unaffected by the vortex street. Only the incoming particle stream between $y_{in} = 0.093$ and $y_{in} = 0.107$ gets involved with the vortex motion behind the cylinder.

5. Quantitative measures of the chaotic saddle

Up to now we have only investigated the topological structure of the system. Next let us briefly consider a few quantitative properties of the chaos.

When a chaotic saddle Λ is purely hyperbolic (i.e. if it does not contain any elliptic periodic orbits and not any KAM tori) then we expect that the relative probability $W(Dt)$ to find a scattering trajectory with a time delay of Dt is given in the limit of large Dt by the exponential law:

$$W(Dt) = \kappa \exp(-Dt \cdot \kappa) \tag{9}$$

κ is the escape rate of Λ [3]. When there are elliptic periodic orbits and KAM tori, then this behaviour is changed to a power law for very large Dt. In our system we did not find elliptic periodic orbits and no large KAM tori. However, we are not able to prove the hyperbolicity of Λ and probably there exist small KAM tori. If these KAM tori are sufficiently small, then they do not have a significant influence on the scattering behaviour and for values of Dt which are not extremely large we expect (9) to hold in good approximation.

To construct figure 8 the following is done: the Dt-axis is cut into boxes of length 0.5, several thousand trajectories with $y_{in} = 0.0995$ and t_{in} distributed evenly have been run and their values of Dt have been monitored and collected into the boxes. In figure 8 the logarithms of the count rates of the various boxes between $Dt = 3.0$ and $Dt = 7.0$ are displayed. The points are located approximately on a straight line with slope -1.4 leading to an estimate of 1.4 for the value of κ. This value is a measure for the effective total instability of Λ. If we are interested in the value of κ related to the stroboscopic map, then we have to multiply the value given above by T_c.

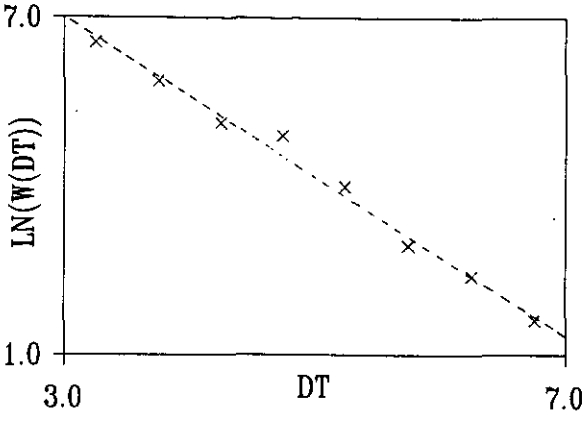

Figure 8. Logarithm of the relative probability for values of Dt. The broken line with slope -1.4 gives the linear approximation to this function.

The number $N(S)$ of disjoint intervals of continuity of $Dt(t_{in})$ which contain any trajectory with $Dt < S$, is expected to behave in the limit of large S like

$$N(S) = \exp(K_0 \cdot S / T_c) \tag{10}$$

where K_0 is the topological entropy of the system [3]. For the validity of (10) analogous restrictions with respect to hyperbolicity hold as the ones for (9). Unfortunately the numerical precision of our computation is not sufficiently good to identify intervals for very high values of S. Therefore we cannot give a precise value for K_0 but only a rough estimate in the order of $K_0 \approx 0.8$.

6. Final remarks

We have analysed a two-dimensional incompressible hydrodynamical system which can visualize the flow in phase space of a Hamiltonian system with one degree of freedom. Because the hydrodynamical system is open, it corresponds to an open Hamiltonian system and the type of chaos which can occur in the explicitly time-dependent case is scattering chaos or transient chaos. In our case the hydrodynamical velocity field is exactly periodic in time and therefore the solution of the Navier–Stokes equation is not chaotic, it is a stable limit cycle. What is chaotic in the hydrodynamical system are the trajectories of passive marker particles. Therefore we encounter a case of Lagrangian turbulence or chaotic advection and because the chaos is transient, we can call this kind of behaviour 'transient Lagrangian turbulence'.

We have based our demonstration on numerical computations and the reader may ask, whether numerical errors have any essential influence on the results. We are confident that the qualitative results do not depend on numerical errors because they have a similar effect to small changes of the system itself and the scenario presented in this paper is structurally stable against small deformations of the system in the following sense: the central point for the existence of topological chaos are the periodic orbits γ and $\tilde{\gamma}$, the corresponding fixed points r and $\tilde{r}$ in the stroboscopic plane and the transversal intersections of their invariant manifolds. Because the eigenvalues μ_i of these fixed points are far away from the unit circle, the periodic orbits do not change

their qualitative properties under small deformations of the system. They will be displaced a little only. Also the invariant manifolds may become deformed, but, most important, the existence of transversal intersections remains. The existence of these intersections is the essential criterion for the creation of topological chaos and in particular for the existence of the chaotic saddle Λ.

The connection between scattering and hydrodynamics opens a new method to investigate the mechanism of scattering chaos in experiment. Vice versa, it allows application of the methods developed for scattering chaos to the analysis of open hydrodynamical systems. This is interesting since experiments on hydrodynamics in a channel containing an obstacle have already been done (for some examples see [17–19]). However, so far these experiments have not yet been analysed and interpreted in terms of scattering chaos.

The phenomenon of chaotic advection may also have a practical applicability: if we have to manage the irregular distribution of a stream of particles injected into a flow, then it is not necessary to make the flow itself turbulent. Even a regular, exactly periodic flow can lead to the desired irregular behaviour of the injected particles. This regular flow can be realized with lower Reynolds numbers and thereby perhaps with smaller effort.

Some readers may find it disturbing that in our model system the asymptotic form of the flow in the channel corresponds to a Hamiltonian whose asymptotic form is

$$H_{as} = u_0 p^2 (0.3 - p)/3 \tag{11}$$

where p is the canonical momentum of the particle. This is not the usual form of the kinetic energy of a particle. However, with a little more effort we can construct a hydrodynamical system, which reproduces the usual form of the kinetic energy of a free particle: let the walls of an empty channel be placed at $y = +D$ and $y = -D$. Let the upper wall move to the right with velocity $u = D/m$ and let the lower wall move to the left with velocity $u = -D/m$. We do not need any further pump for the motion of the fluid. If D/m is not too large, then the velocity field of fluid is given by

$$u(x, y) = y/m \tag{12}$$

$$v(x, y) \equiv 0. \tag{13}$$

The corresponding ψ function has the form

$$\psi(x, y) = y^2/2m. \tag{14}$$

This is the usual form of the kinetic energy if we identify as before y with the momentum of the particle, m with its mass and ψ with the Hamiltonian function. Next let D be sufficiently large and place an obstacle with size small compared to D into the middle of the channel. This causes a modification of ψ in the vicinity of the obstacle and we can interpret this modification of ψ which depends on y, x and possibly on t as a localized interaction part of the Hamiltonian. In this way it is possible to simulate a Hamiltonian scattering system with the usual asymptotic structure.

Acknowledgment

One of the authors (CJ) thanks the Deutsche Forschungsgemeinschaft for financial support in form of a Heisenberg stipendium. The fluid dynamical computer program was constructed originally for the Priority Project 'Finite Approximations in Fluid

Dynamics' under the leadership of professor E Krause. One of the authors (EZ) thanks the Deutsche Forschungsgemeinschaft for financial support and professor E Krause for his help within this project. The computations have been done on the vector computer Cyber 205 of the Computer Centre of the University Bochum. We thank the staff of the Computer Centre and Dr R Mannshardt for their support.

References

[1] Eckhardt B 1988 *Physica* **33D** 89
[2] Smilansky U 1990 *Course X of the Les Houches Session LII* ed M Giannoni, A Voros and J Zinn-Justin (New York: Elsevier)
[3] Tel T 1990 *Directions in Chaos* vol 3 ed B Hao (Singapore: World Scientific) pp 149–221
[4] Aref H 1984 *J. Fluid Mech.* **143** 1
[5] Chaiken J, Chu C K, Tabor M and Tan Q M 1987 *Phys. Fluids* **30** 687
[6] Jones S and Aref H 1988 *Phys. Fluids* **31** 469
[7] Jones S, Thomas O and Aref H 1989 *J. Fluid Mech.* **209** 335
[8] Eckhardt B and Jung C 1986 *J. Phys. A: Math. Gen.* **19** L829
[9] Jung C and Scholz H J 1987 *J. Phys. A: Math. Gen.* **20** 3607
[10] Jung C and Scholz H J 1988 *J. Phys. A: Math. Gen.* **21** 2301
[11] Jung C 1991 *The Electron* ed D Hestenes and A Weingartshofer (Dordrecht: Kluwer)
[12] Harlow F H and Welch J E 1965 *Phys. Fluids* **8** 2182
[13] Guckenheimer J and Holmes P 1983 *Nonlinear Oscillations, Dynamical Systems and Bifurcations of Vector Fields* (New York: Springer)
[14] Ottino J 1989 *The Kinematics of Mixing: Stretching, Chaos and Transport* (Cambridge: Cambridge University Press)
[15] Aref H 1990 *Phil. Trans. R. Soc. London* **333** 273
[16] Ottino J 1990 *Ann. Rev. Fluid Mech.* **22** 207
[17] Van Dyke M 1982 *An Album of Fluid Motion* (Stanford: The Parabolic Press)
[18] Tamura T, Krause E, Shirayama S, Ishii K and Kuwahara K 1988 *Proc. 11th Int. Conf. on Numerical Methods in Fluid Dynamics (Williamsburg)*
[19] Wang X and Dalton C 1990 *Proc. Int. Symp. Non-steady Fluid Dynamics* ASME Toronto